nature portfolio

https://doi.org/10.1038/s41586-024-07467-0

Supplementary information

The time between Palaeolithic hearths

In the format provided by the authors and unedited

Supplementary Information for

The time between Paleolithic hearths

Ángela Herrejón-Lagunilla[1,2*], Juan José Villalaín[1], Francisco Javier Pavón-Carrasco[2,3], Mario Serrano Sánchez-Bravo[2,3], Santiago Sossa-Ríos[4], Alejandro Mayor[5], Bertila Galván[6], Cristo M. Hernández[6,7**], Carolina Mallol[6,7,8**], Ángel Carrancho[9**].

[1] Área de Física Aplicada, Departamento de Física, Universidad de Burgos; Burgos, Spain.

[2] Departamento de Física de la Tierra y Astrofísica, Facultad de Ciencias Físicas, Universidad Complutense de Madrid; Madrid, Spain.

[3] Departamento de Dinámica Terrestre y Observación de la Tierra, Instituto de Geociencias, Consejo Superior de Investigaciones Científicas-Universidad Complutense de Madrid; Madrid, Spain.

[4] Àrea de Prehistòria; Departament de Prehistòria, Arqueologia i Història Antiga, Facultat de Geografia i Història, Universitat de València; València, Spain.

[5] Àrea de Prehistòria, Departament de Prehistòria, Arqueologia, Història Antiga, Filologia Llatina i Filologia Grega, Facultat de Filosofia i Lletres, Universitat d'Alacant; Sant Vicent del Raspeig, Spain.

[6] Área de Prehistoria, Unidad de Docencia e Investigación de Prehistoria, Arqueología e Historia Antigua, Departamento de Geografía e Historia, Facultad de Humanidades, Universidad de La Laguna; San Cristóbal de La Laguna, Tenerife, Spain.

[7] Archaeological Micromorphology and Biomarkers Laboratory, Instituto Universitario de Bio-Orgánica Antonio González, Universidad de La Laguna; San Cristóbal de La Laguna, Tenerife, Spain.

[8] Department of Anthropology, University of California, Davis, California, United States.

[9] Área de Prehistoria, Departamento de Historia, Geografía y Comunicación, Universidad de Burgos; Burgos, Spain.

*Corresponding author.

Email: aherrejon@ubu.es

**Equal contribution

Index of contents

Supplementary Note 1. El Salt unit X

El Salt is located in Alcoi (Alacant, Eastern Spain; Fig. 1), close to the confluence of Polop and Barxell rivers. It is an open-air site at 680 meters above the sea level comprising a 4-meter-thick sedimentary deposit at the foot of a 38-meter-tall Paleocene limestone cliff draped by Pleistocene travertine (Extended data Fig. 1)[34-36, 50].

The stratified sedimentary sequence at El Salt is divided into 13 lithostratigraphic units, grouped according to their texture and archeological content[34-36]. Unit X is included in a group (from Unit XII to IX) characterized by silty/sandy-silty sediments. This group of units rests on a series of large, fallen limestone blocks resting directly on Unit XIII[50]. The age of these units X- XII is estimated around the start of MIS 3, before Heinrich Event 5 (50-47 ka BP)[17]. Unit X was subdivided in two subunits (Xa and Xb) according to color and texture: Xa is sandier and its color is lighter, while Xb is clayier and darker[20, 50-51]. In the horizontal dimension, Unit X is divided in two different parts: an outer and an inner part (Extended data Fig. 1c). The outer part is characterized by sedimentary homogeneity and presents fewer anthropogenic inputs. The inner part, closer to the wall, displays more complex sedimentary features, with interstratification of different sedimentary facies and abundant anthropogenic inputs (Extended data Fig. 1c).

Supplementary Note 2. Archeostratigraphic inferences

The following inferences were made based on the archeostratigraphic analysis of the lithic, faunal and combustion remains:

-1) The position of bed 4 in contact with the H48 black layer and above H59 indicates that the former hearth is more recent than the latter (Fig. 1e).

-2) H50 is the only hearth from the outer area with a well-preserved ash layer, which is stratigraphically associated with the archeological remains from beds 8-10 (Fig. 1d). Furthermore, the top of H50 is located below beds 6-7 (Fig. 1d).

-3) The hearths from the outer area are stratified as follows: H48 at the top, H59 in the middle and H50 at the base.

-4) The hearths from the inner area (H57 and H55) both display a well-preserved ash layer. The H57 ash layer and stratigraphically associated materials are located at the top of the studied sequence within subunit Xb, and just above bed 2-5.1 (Fig. 1c). For H55, the ash layer and associated materials overlap with bed 2-5.2 and show a horizontal association with bed 2-5.1 (Fig. 1c). Thus, H57 is more recent than H55.

Supplementary Note 3. Differences in the reversibility of the thermomagnetic curves of white and black layers

Rock magnetic experiments provide additional information about the burning conditions undergone by the hearths. White layer samples exhibit highly reversible curves (coinciding heating and cooling curves) up to 700 ºC (Extended data Fig. 6a-c). This thermochemical stability is coherent with the high temperatures observed in similar studies on archeological and experimentally produced ashes[31, 43, 52]. On the contrary, the underlying black layer samples show irreversible curves due to the neoformation of secondary magnetite during experimental lab heating (Extended data Fig. 6d-f). This indicates that black layers reached lower temperatures than those applied in the laboratory (700 ºC), which is also coherent with the behavior observed in previous works on analogous materials[31, 52-53]. Rock-magnetic results (partial thermomagnetic curves) obtained on black layer samples suggest maximum heating temperatures of around 450–500 ºC. This agrees well with micromorphological and mineralogical observations on black layers from El Salt site[19].

Supplementary Methods 1. Specimens' selection for calculating mean archeomagnetic directions

For H50, we had to exclude all the specimens obtained from three of the archeomagnetic (oriented) blocks with burnt sedimentary facies. Two of them (blocks C3 and C4) were damaged and/or affected by rain during the sampling process. These blocks were soaked prior to plastering and cracked areas were observed. This implies local mechanical alterations. As expected, anomalous results were obtained, showing deviated and highly scattered directions. Even in the cases where the direction is more or less northward, we cannot exclude a bias due to the mentioned damage. For this reason, the blocks were excluded as a precaution. Block C1, containing exclusively white layer, was also excluded. Considering that white layer reaches higher temperatures than black layers during the heating, the ChRM component (related to heating) in the C1 specimens was isolated between 200-300 ºC and 500-600 ºC (Extended data Fig. 9a). They are systematically of normal polarity. Contrary to most thermally altered substrate (black layer) specimens (Extended data Fig. 8), a single, progressive intensity decay was observed in all the specimens from this block. This evidence points to the existence of a single component related to fire, which implies that in these specimens, the magnetization mechanism is most likely a full thermoremanence (TRM). When calculating the mean direction of this component, we observed a suspicious behavior. Declination showed similar values to those observed in accepted specimens from other H50 blocks. However, the inclination was clearly lower (Extended data Fig. 9b). This is possibly a flattening effect due to the compaction of ashes after the fire. Experimental work has shown that ashes, due to their unconsolidated nature, are highly volatile and particularly prone to be reworked after heating[31].

Specimens from the archeomagnetic oriented blocks C1, C3 and C4 (all from hearth H50) are not included in the total number of samples in Table 1.

Apart from the exceptions mentioned, two filtering steps were established for the selection of specimens considered for the calculation of mean directions:

1) First, all specimens with a maximum angular deviation (MAD) > 5.0 º were excluded.
2) Subsequently, the mean direction of the hearth was recalculated and all specimens with a direction deviated by more than 25.0º with respect to the mean direction were excluded.

After applying these criteria, the mean archeomagnetic directions were calculated (Table 1 and Extended data Fig. 7). H57 has not been used because it is considered that it does not meet minimum acceptance criteria for our purposes (N>6 specimens; k>50; α_{95}<10.0º).

Supplementary Methods 2. Estimation of minimum times necessary to explain the angular deviation between directions within pairs of hearths according to SV.

The calculation is divided into several steps:

***Step 1.* Probability density distribution (PDF) for the angular deviation between each pair of archeomagnetic directions.**

An archeomagnetic direction is given by the declination (D) and inclination (I) angles and by the directional error α_{95} at 95% of confidence. It is assumed that this direction and its error follow a spherical Fisher distribution (see [41,54] for more details). The mean angular deviation Ω between two directions (D_1, I_1 and D_2, I_2) can be estimated using the next expression:

$$\Omega = acos[cosI_1 \cdot cosI_2 \cdot cos(D_1 - D_2) + sinI_1 \cdot sinI_2] \quad [1]$$

However, if we want to estimate not only the mean angular deviation but also its statistical distribution (also known as Probability Density Function - PDF), we need to consider the angles α_{95} for each direction (i.e., $\alpha_{95.1}$ and $\alpha_{95.2}$).

To do that, we first generate two sets of synthetic declinations and inclinations data (10^8 data for each set) for each direction by means of the Fisher statistic[41]. Then, we calculate the angular deviation Ω between all the 10^8 pairs of random synthetic data. The normalized histograms provide the PDF for the angular deviation between each pair of directions.

Supplementary Figure 1 shows the final PDF for each pair of archeomagnetic directions. The maxima in those PDFs correspond to the most probable angular deviation Ω between two pairs of directions.

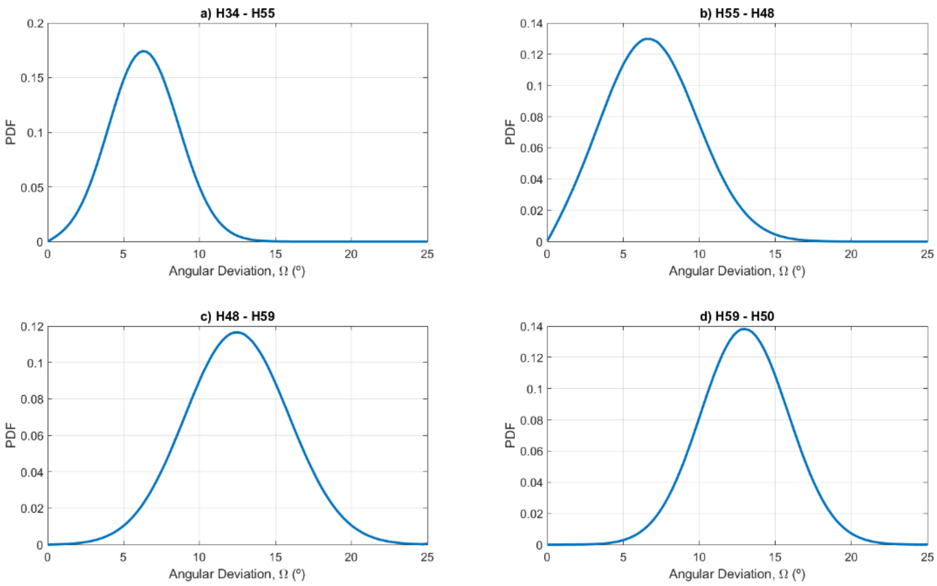

Supplementary Figure 1. *PDF for the angular deviation Ω between each pair of archeomagnetic directions: A) H34-H55, B) H55-H48, C) H48-H59, D) H59-H50. Each graphic was done with a sampling of 10^{-8} pairs of directions.*

***Step 2.* Probability density distribution (PDF) for the minimum elapsed time Δt_{min} given a critical angular deviation Ω_C.**

In this step, we estimate the probability density distribution (PDF) of the minimum elapsed time Δt_{min} required to reach a specific angular deviation Ω using a reference PSVC. This procedure is carried out considering a critical angular deviation Ω_C running from 1º up to 25º (in steps of 1º). In other words, we estimate all the possible minimum elapsed times between two pairs of directions characterized by a constant angular deviation of Ω_C.

Just an example: for a certain time within the selected time window, we get from the PSVC the declination and inclination values (yellow stars in Supplementary Figure 2a and b). Then, we calculate the angular deviation between this direction and the rest of the directional data contained in the PSVC (Supplementary Figure 2c). As expected, the curve of the angular deviation presents an absolute minimum of 0º at the time of the chosen data (yellow star in Supplementary Figure 2c and in zoom of Supplementary Figure 2d). Finally, we estimate the minimum elapsed time Δt_{min} necessary to reach the critical angular deviation of 5º in both time directions (in this strategy, we are indifferent to the direction of time's progression, be it forward or backward). After applying this approach to the total number of directional data of the PSVC, we obtain a set of characteristic Δt_{min} for the Ω_C = 5º. The set of Δt_{min} can be represented in a histogram that shows they are not randomly distributed but instead follow a characteristic statistical distribution (Supplementary Figure 2e).

This example is repeated for Ω_C ranging from 1º to 25º and using the PSVCs of the two paleoreconstructions and the *toy-model*. It is important to note that the role of the PSVC is a key point since it provides synthetic directional data. For this reason and so that we can demonstrate that our technique is robust enough, we have used different PSVCs coming from two global archeomagnetic models. In addition, we have also developed a case study of synthetic PSVCs from the *toy-model* that support our results.

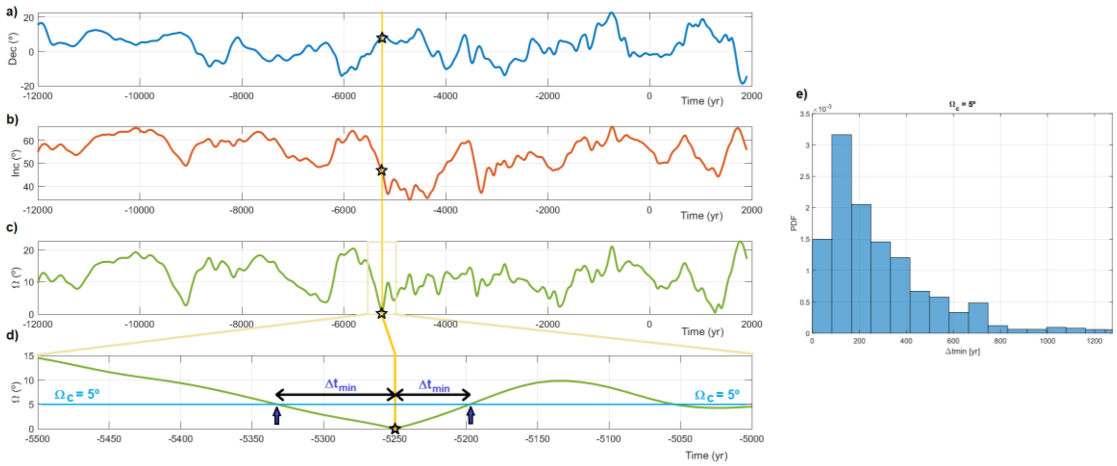

Supplementary Figure 2. *Example of how to get a distribution of the minimum elapsed time Δt_{min} for a critical angular deviation Ω_c = 5º. a) and b) Declination and inclination PSVCs, respectively (based on SHA.DIF.14k reconstruction). The yellow star indicates the directional data for a chosen time. c) Angular deviation between the selected directional data (yellow stars in a) and b)) and the rest of the directional data contained in the PSVC. d) Zoom (around the chosen time) of the angular deviation showing the minimum elapsed time necessary to reach in both time directions, and for the first time, the critical angular deviation Ω_c. e) Histogram of a set of Δt_{min} obtained after applying the approach to the total number of data of the PSVC (27454 pairs of directions for Ω_c = 5º).*

a) PDF of the Δt_{min} using the global archeomagnetic reconstructions.

We used two different PSVCs at El Salt coordinates coming from the following archeomagnetic models: SHA.DIF.14k[27] and ARCHKALMAG14k[28]. We have used these models since they are the available models based only on TRM data that cover the largest time interval (with both models spanning over the last 14 kyr). Supplementary Figure 3 shows the directional PSVCs for the two models at El Salt coordinates.

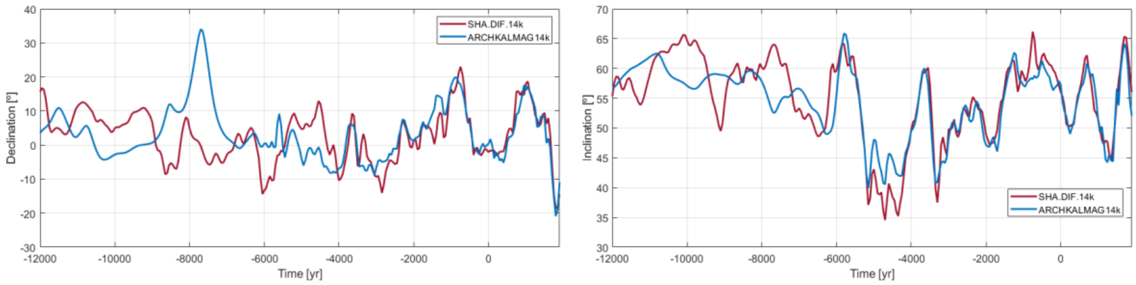

Supplementary Figure 3. *Directional PSVCs (left declination and right inclination) at El Salt coordinates for the used archeomagnetic global models SHA.DIF.14k (red) and ARCHKALMAG14k (blue).*

Using these curves, we have calculated the PDF for the Δt_{min} considering a set of angular deviations Ω_C ranging from 1º to 25º. Some examples (for different Ω_C) of these normalized histograms (PDF) are shown in Supplementary Figure 4 for the two different archeomagnetic models.

For each normalized histogram we have estimated the best statistical distribution that fits the histogram. The best distribution function is the log-normal distribution (we have tried with several distributions, and this one is the best option). The log-normal distribution fits the data following the next equation:

$$f(x;\mu,\sigma) = \frac{1}{x\sigma\sqrt{2\pi}} exp\left(-\frac{(lnx-\mu)^2}{2\sigma^2}\right) \quad [2]$$

where μ (mean of the variable's natural logarithm) and σ (standard deviation of the variable's natural logarithm) are the parameters of the distribution. For each normalized histogram, we obtain the μ and σ parameters. With these parameters, we obtain the log-normal PDF for each histogram. The PDFs for some critical angular deviation values are plotted in Supplementary Figure 4 as a red line. In Supplementary Table 1 we provide the values of these parameters for each Ω_C and for each archeomagnetic model.

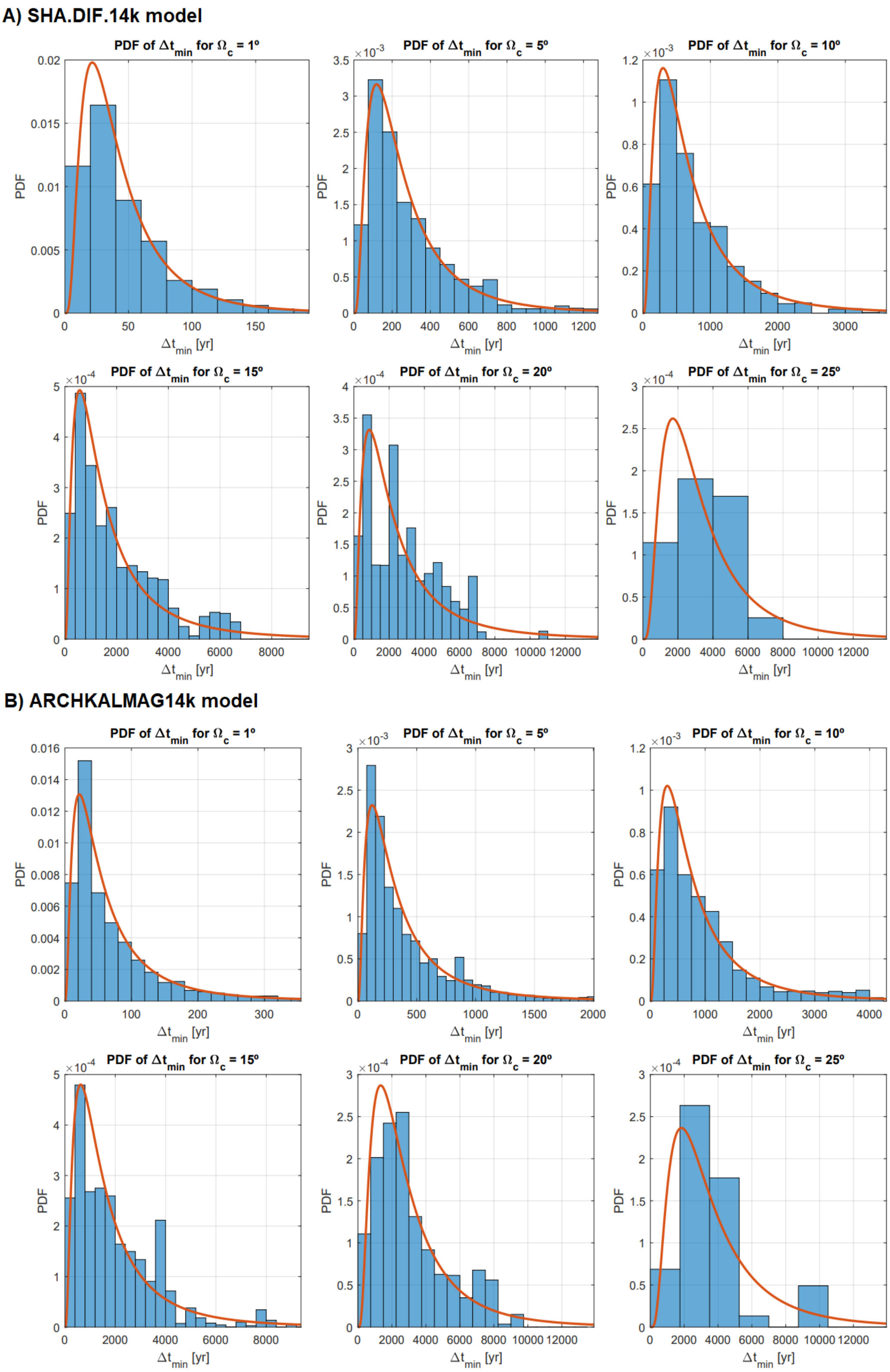

Supplementary Figure 4. *Normalized histogram (PDF) of the* Δt_{min} *for different critical angular deviation values (blue histograms). Red lines represent the log-normal PDF curves. Panel A: SHA.DIF.14k, panel B: ARCHKALMAG14k. [Total number of pairs of directions considered for the histograms: 27769 pairs for* Ω_C*=1º, 27454 pairs for* Ω_C*=5º, 25298 pairs for* Ω_C*=10º, 21059 pairs for* Ω_C*=15º, 14343 pairs for* Ω_C*=20º, 7401 pairs for* Ω_C*=25º in the case of SHA.DIF.14k; 27752 pairs for* Ω_C*=1º, 26906 pairs for* Ω_C*=5º, 23839 pairs for* Ω_C*=10º, 21961 pairs for* Ω_C*=15º, 14158 pairs for* Ω_C*=20º, 2412 pairs for* Ω_C*=25º in the case of ARCHKALMAG14k]*

	SHA.DIF.14k		ARCHKALMAG14k		Toy-model	
Ω_C	μ	σ	μ	σ	μ	σ
1	3.589	0.721	3.925	0.922	3.295	0.578
2	4.306	0.762	4.634	0.933	3.994	0.593
3	4.758	0.790	5.085	0.961	4.435	0.607
4	5.097	0.795	5.390	0.926	4.785	0.624
5	5.388	0.783	5.652	0.925	5.064	0.633
6	5.638	0.785	5.844	0.909	5.307	0.653
7	5.851	0.777	6.068	0.917	5.521	0.672
8	6.065	0.784	6.222	0.905	5.752	0.705
9	6.232	0.794	6.353	0.883	5.945	0.741
10	6.373	0.821	6.487	0.868	6.175	0.783
11	6.511	0.854	6.625	0.858	6.355	0.816
12	6.676	0.874	6.774	0.866	6.572	0.866
13	6.862	0.900	6.952	0.882	6.815	0.911
14	7.022	0.922	7.114	0.894	6.976	0.945
15	7.203	0.924	7.235	0.892	7.177	0.960
16	7.338	0.927	7.399	0.887	7.317	0.977
17	7.437	0.931	7.548	0.866	7.434	0.973
18	7.520	0.942	7.653	0.837	7.519	0.970
19	7.583	0.937	7.717	0.801	7.622	0.970
20	7.602	0.911	7.795	0.770	7.744	0.939
21	7.637	0.891	7.818	0.779	7.821	0.946
22	7.714	0.841	7.783	0.795	7.811	0.960
23	7.767	0.813	7.779	0.812	7.837	0.891
24	7.849	0.770	7.812	0.822	7.932	0.894
25	7.931	0.698	8.023	0.713	7.965	0.898

Supplementary Table 1. *Values of the log-normal parameters for each Ω_C and for each archeomagnetic model and the toy-model.*

b) PDF of the Δt_{min} using the *toy-model*.

Additionally, we have generated synthetic PSVCs, which we refer to as *toy-model*. These are based on the temporal characteristics given by the archeomagnetic models, specifically by synthesising the PSVC provided by the ARCHKALMAG14k model at El Salt coordinates. The purpose of generating this *toy-model* is to test the robustness of our results when using the archeomagnetic paleoreconstructions, taking into account their inherent limitations. These paleoreconstructions have a limited temporal range (14 kyr), which consequently restricts the number of direction pairs that can be compared. This could lead to Δt_{min} histograms that may not be robust enough to accurately define the log-normal PDFs, especially for large values of Ω_C (see Supplementary Figure 4). By creating this *toy-model*, we can generate as many directional pairs as needed to adequately define the PDFs, even for large values of Ω_C.

The set of synthetic PSVCs was generated by directly synthesizing the PSVC characteristics given by the ARCHKALMAG14k at El Salt coordinates over the last 4 kyr. We only chose this 4 kyr time interval as it is the most well-defined interval supported by data, thereby minimizing potential smoothness in field variations due to limited information from earlier periods (see [27, 28] for details). We synthesized these PSVCs by directly assimilating the actual PSVC described by the ARCHKALMAG14k into autoregressive models for both, the temporal evolution of declination (*D*) and inclination (*I*) at El Salt coordinates. Given a knot space of 50 yr for describing the evolution of the ARCHKALMAG14k PSVC, we have approximated the evolution of the synthetic PSVCs by an autoregressive model of order 2 (order based on the characteristics of the autocorrelation and partial autocorrelation functions):

$$D_t = c_D + a_1 D_{t-1} + a_2 D_{t-2} + \varepsilon_{D_t} \qquad [3]$$

$$I_t = c_I + b_1 I_{t-1} + b_2 I_{t-2} + \varepsilon_{I_t} \qquad [4]$$

where c_D and c_I are constant values; a_i and b_i are parameters that relate the value of declination or inclination at a certain time (D_t or I_t) with their values at previous knot times (i.e., 50 yr before for D_{t-1} and I_{t-1}, and 100 yr before for D_{t-2} and I_{t-2}); ε_{D_t} and ε_{I_t} are white noise terms that incorporate the stochastic nature of the time evolution of the geomagnetic field into this *toy-model*. The value of these parameters is estimated by fitting the PSVC of the ARCHKALMAG14k using maximum likelihood. Then, we can create synthetic PSVCs simulations by setting initial values for declination and inclination.

This method allows us to generate synthetic PSVCs at El Salt coordinates that show similar properties (similar temporal characterization and amplitude) of the declination and inclination elements of those given by the PSVC of the paleoreconstructions (Supplementary Figure 5). In accordance with the time span of the selected paleoreconstructions, we generated our *toy-model* to also span for 14 kyr. Since this target time window spans more than 10 kyr, the Geocentric Axial Dipole (GAD) hypothesis must be satisfied. In order to show that the toy-model satisfies the mentioned GAD hypothesis (i.e., mean declination close to 0° and mean inclination close to $tan^{-1}(2 \cdot tan(latitude_{Salt})) \approx 58°$), we have plotted in Supplementary Figure 6 a set of 1000 PSVCs along with their respective total mean values (yellow lines). As expected, the toy-model satisfies the GAD hypothesis.

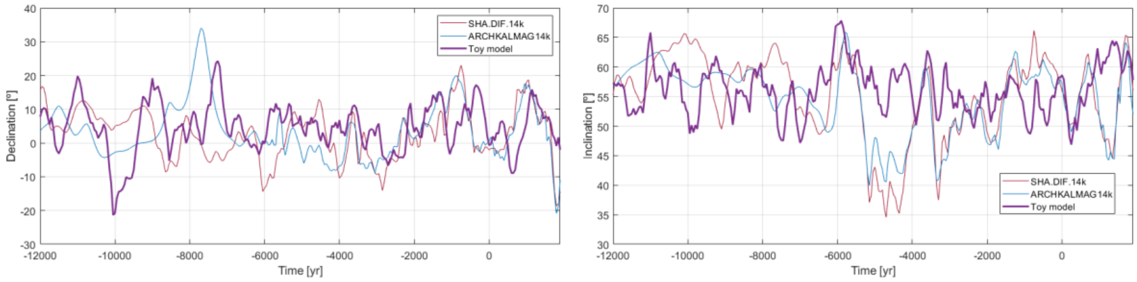

Supplementary Figure 5. *Example (violet curves) of PSVC generated by using the toy-model (left declination and right inclination). For comparison, the PSVCs given by the paleoreconstructions are plotted with the same color pattern used in Supplementary Figure 3.*

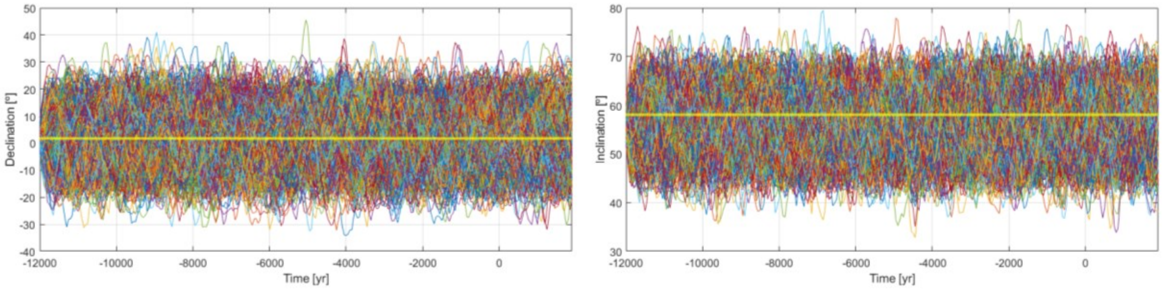

Supplementary Figure 6. *1000 PSVCs generated by using the toy- model (left declination and right inclination). Yellow lines show the mean value of the different declination and inclination curves.*

As for the case "a) PDF of the Δt_{min} using the global archeomagnetic reconstructions", we obtain normalized histograms for the minimum elapsed time from the synthetic directions separated by a critical angular deviation Ω_C using the PSVCs generated by the *toy-model*. In this case, to better define the histograms for each Ω_C, instead of using a single PSVC (as the case of the paleoreconstructions), we take advantage of the *toy-model* generating 1000 PSVCs at El Salt coordinates. These normalized histograms are plotted in Supplementary Figure 7. In addition, for each histogram, we also calculate the log-normal distributions (red lines in Supplementary Figure 7). As can be seen, these PDFs are much better defined than those obtained with the paleoreconstructions, specially for the largest values of Ω_C.

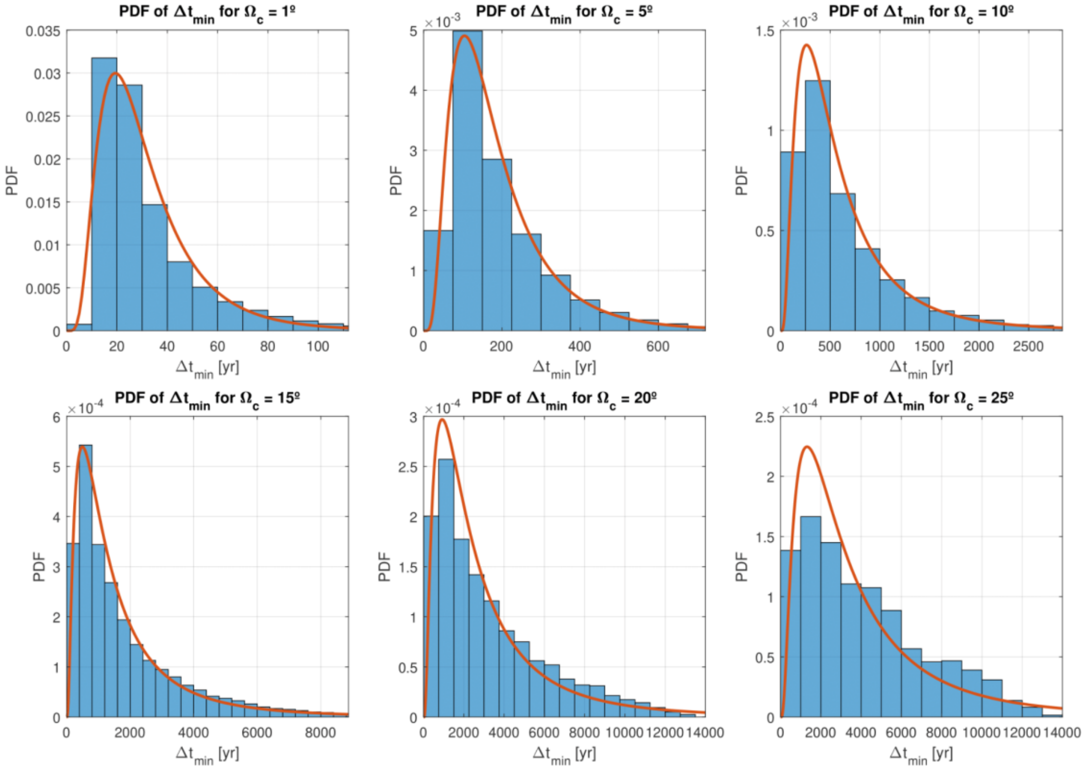

Supplementary Figure 7. *Normalized histogram (PDF) of the Δt_{min} for different critical angular deviation values (blue histograms). Red lines represent the log-normal PDF curves. [Total number of pairs of directions considered for the histograms: 2794328 pairs for Ω_C=1º, 2759364 pairs for Ω_C=5º, 2645079 pairs for Ω_C=10º, 2158415 pairs for Ω_C=15º, 916719 pairs for Ω_C=20º, 189321 pairs for Ω_C=25º]*

Step 3. ***Combination of the PDF of Step 1 with the PDFs of Step 2.***

On one hand, the PDF of step 1 (henceforth PDF1) provides the probability distribution for the angular deviation Ω between the two archeomagnetic directions. The PDFs (PDF1) of the four pairs of directional data of El Salt are given in Supplementary Figure 1. On the other hand, the log-normal PDFs of step 2 (henceforth PDF2) provide the probability of distribution for the minimum elapsed time Δt_{min} for a given angular deviation Ω_C between directions obtained from a reference PSVC (with Ω_C ranging from 1º to 25º, in steps of 1º). A set of some PDF2 for some angular deviation values (Ω_C = 1, 5, 10, 15, 20, 25º) are plotted in Supplementary Figure 8. This figure shows how the PDF2 from the different models present similar results. For lower angular deviations (Ω_C < 15°), the PDF2s of the Toy-model present narrower shapes around the maximum than the PDF2s of the archeomagnetic models. This is expected, since the Toy-model was developed using only the directional information of the ARCHKALMAG14k model for the last 4 kyr, period well-constrained by the data and thus providing higher directional variability (i.e. for a given Δt_{min}, lower elapsed times are expected). However, for angular deviation higher than 15° all the PDF2s present similar results. In fact, for the critical angular deviation of 15º, all the PDF2s agree themself. The similarities between the PDF2s of the Toy-model and the paleoreconstructions for large values of Ω_C support the reliability of the PDF2s for the paleoreconstructions within these large Ω_C values, where the histograms of Δt_{min} are not clearly defined (see Supplementary Figure 4).

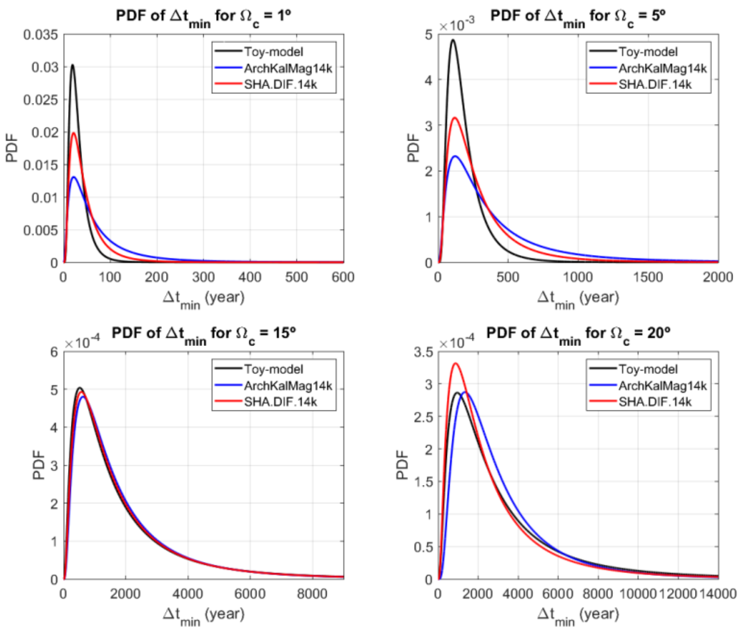

Supplementary Figure 8. *PDF of the* Δt_{min} *for different critical angular deviations and for the two paleoreconstructions and the toy-model. (These graphics are based on the histograms represented in Supplementary Figures 4 and 7; total number of pairs of directions considered for the histograms are indicated in the captions of those figures)*

To get the final PDF corresponding to the minimum elapsed time between the pair of two archeomagnetic directions, we have to combine both PDFs, i.e. the PDF1 (that only depends on the angular deviation) with each PDF2 (that depends on the angular deviation and time). Since the PDF1 is related to the angular deviation and the second set of PDFs (PDF2) provides the probability of the minimum elapsed time for different angular deviation values, we have to calculate the final PDF following the next combination:

$$PDF_{combined}(t) = \frac{\sum PDF1(\Omega)\cdot PDF2(t,\Omega)}{\sum PDF1(\Omega)}$$

where the summation is extended up to $\Omega = 25°$.

Using the combined PDF we can establish the minimum elapsed time Δt_{min} between both pairs of directional data at a certain probability. In details, we can estimate the most often value of Δt_{min} (mode of the combined PDF) or its values at 68% or 95% of confidence level. For a combined PDF, the estimation of Δt_{min} for a certain level of confidence (in terms of % of probability) is calculated as follows. The Δt_{min} (for a given confidence level) is calculated when the area under the PDF curve reaches the chosen probability within the interval $[\Delta t_{min}, \infty)$. To illustrate this calculation, we provide an example using the first pair of directional data from El Salt, denoted as H34 – H55. The combined PDF for this data pair is plotted in Supplementary Figure 9. If one wants to estimate the Δt_{min} for this pair of directional data at, for example, 75% of probability, we need to find the value of Δt_{min} within the PDF such that the area under the curve in the interval [Δt_{min}, ∞) is equal to 0.75 (see Supplementary Figure.9). It is important to note that all the PDFs are normalized distributions, meaning that 75% probability corresponds to an area equal to 0.75. The Δt_{min} that satisfies this condition is Δt_{min} = 175 yr This implies that if we were to examine 100 possible minimum elapsed times in our paleosecular variation curves, corresponding to the angular deviation provided by the data pair, 25 of them would have Δt_{min} less than 175 years, while 75 of them would have Δt_{min} greater than 175 years.

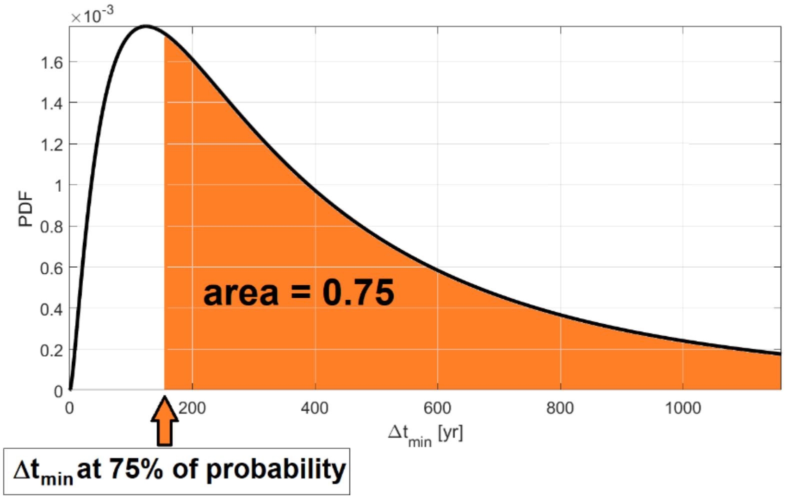

Supplementary Figure 9. *Combined PDF for the El Salt pair H34 – H55 considering the ARCHKALMAG14k model. The orange area corresponds to the 75% of the total area under the PDF (the total area is 1). The orange arrow indicates the* Δt_{min} *needed to get this area (in this case,* Δt_{min} *= 175 yr).*

Supplementary Figure 10 shows the combined PDF for Δt_{min} of the four pairs of directional data from El Salt considering the two archeomagnetic models and the *toy-model*. The vertical lines in each combined PDF show the different probabilities for Δt_{min}. The Extended data Table 1 contains a summary with the final results at different confidence levels, i.e. the minimum time interval Δt_{min} that is necessary to explain the angular deviation Ω between two archeomagnetic directions at El Salt site.

All the calculations mentioned in Supplementary Methods 2 were performed using a custom code generated with Matlab (see Code Availability Statement).

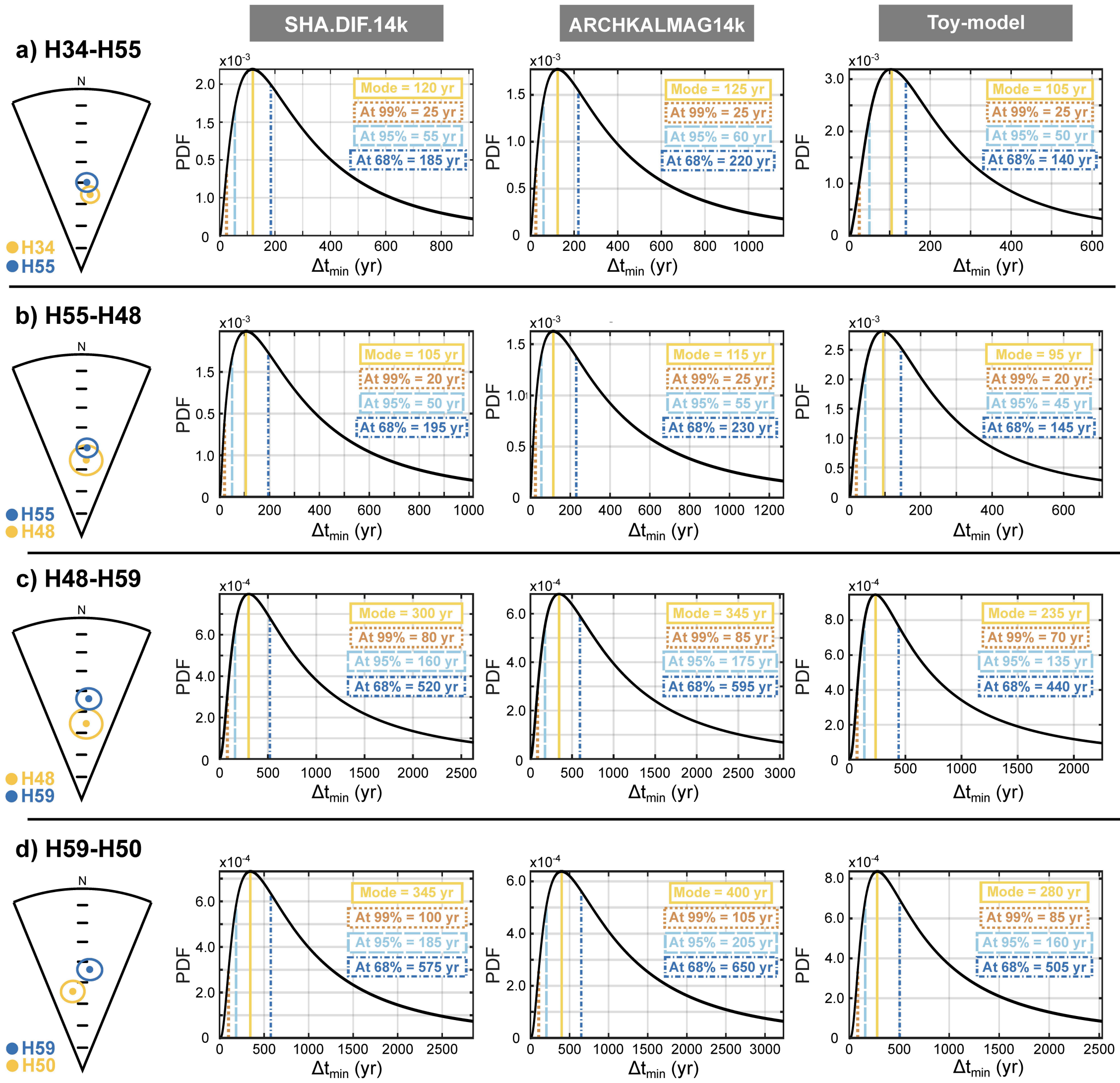

Supplementary Figure 10. *Estimation of the minimum time difference between the last burning of pairs of stratigraphically consecutive hearths: A) H34-H55, B) H55-H48, C) H48-H59, D) H59-H50. From left to right: (1) Equal Area projection with the mean directions (and their respective circle of confidence at 95% probability [p = 0.05] or* α_{95}*) of the compared hearths [calculations of mean directions are based on Fisher's statistics*[41]*; for more details about the number of specimens/samples and statistics, see Extended Data Fig. 7 and Table 1, and their respective captions]; (2,3,4) Temporal estimations according to SHA.DIF.14k, ARCHKALMAG14k, and toy model, respectively. The dark blue, light blue, brown and yellow lines represent the* Δt_{min} *with 68%, 95%, 99% of confidence levels and mode, respectively.*

Supplementary Methods 3. Method validation and limitations.

This section presents diverse case studies incorporating both geomagnetic data and archeomagnetic data. These case studies allow us to get more information about the validation and limitation of the presented method. We propose four case studies covering all the possible scenarios associated with the minimum elapsed time between two directional archeomagnetic data:

- **Case 1. Using geomagnetic data.**
- **Case 2. Impact of the directional error (α_{95}) on the estimation of the Δt_{min}.**
- **Case 3. Using archeomagnetic data with good time control and different ages.**
- **Case 4. Using archeomagnetic data of the same age context.**

Finally, we include a subsection in which we summarize the limitations and instructions to be taken into account when using the method.

Case 1. Using geomagnetic data. We have used historical and instrumental geomagnetic directions at the El Salt coordinates to evaluate the method by means of the historical geomagnetic model GUFM1[55] and the last IGRF-13 model[56]. Supplementary Figure 11 and Supplementary Table 2 contain the values of declination and inclination at the El Salt site for different times covering the last 300 years according to the cited models. Data after 1900 come from the IGRF-13, while data before that epoch are synthesized using the GUFM1, the geomagnetic field model available for the last centuries.

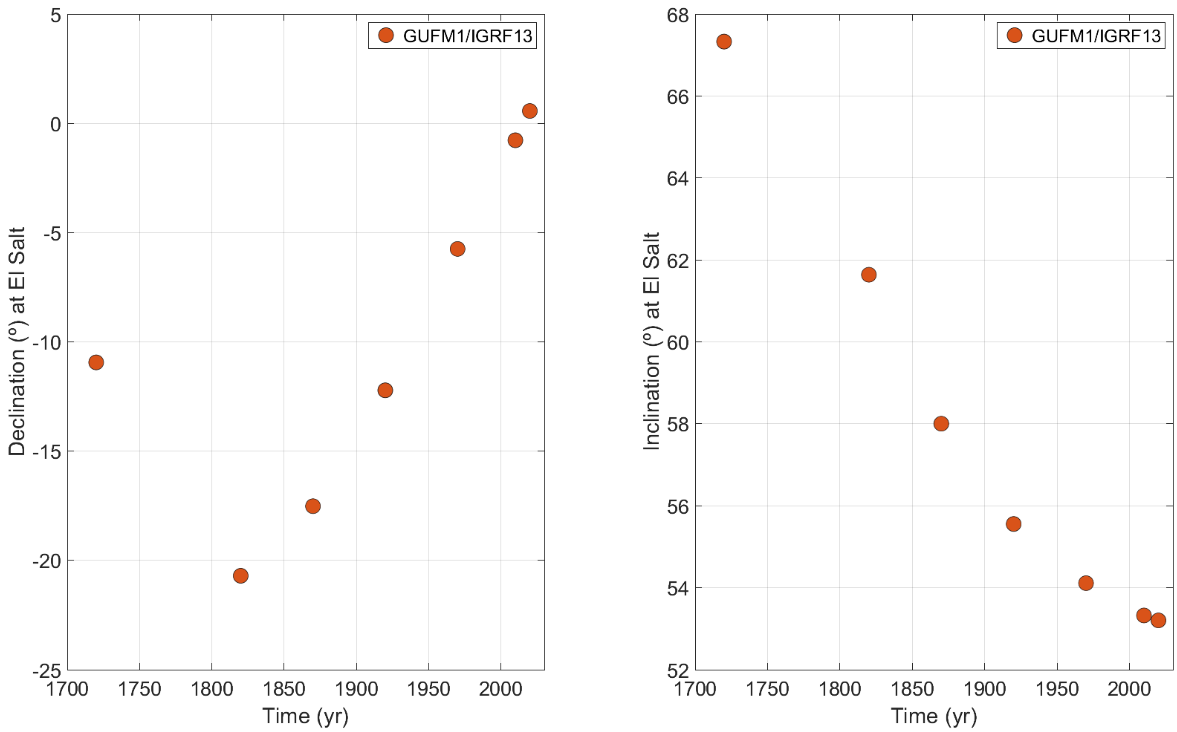

Supplementary Figure 11. *Declination (left panel) and inclination (right panel) at El Salt coordinates according to the models GUFM1 (before 1900) and IGRF-13 (after 1900).*

Time (yr)	Declination (º)	Inclination (º)
2020	0.6	53.2
2010	-0.8	53.3
1970	-5.7	54.1
1920	-12.2	55.6
1870	-17.5	58.0
1820	-20.7	61.6
1720	-10.9	67.3

Supplementary Table 2. *Declination and inclination data at the El Salt coordinates given by the GUFM1 model (data before 1900) and the IGRF-13 (data after 1900 to the present).*

These data provide six pairs of directional data to test the method. Considering the most recent data (at 2020) as a reference direction, the six pairs of data are: *pair 1*: 2020 – 2010; *pair 2*: 2020 – 1970; *pair 3*: 2020 – 1920; *pair 4*: 2020 – 1870; *pair 5*: 2020 – 1820; *pair 6*: 2020 – 1720. For each pair of data, we have applied the method to estimate the minimum elapsed time between both directions. After that, we have compared the results with the real elapsed time for each pair of data (*pair 1*: 10 yr; *pair 2*: 50 yr; *pair 3*: 100 yr; *pair 4*: 150 yr; *pair 5*: 200 yr; *pair 6*: 300 yr). In this first case study, the set of data represents the "true" geomagnetic field during the last centuries and any angular error has been considered (i.e., α_{95} = 0º for all directions). The impact of α_{95} on the method is analyzed in the following Case 2.

Results are shown in Supplementary Table 3. We include the real elapsed time, the angular deviation given by each pair of directions, and the estimated minimum elapsed time Δt_{min} given by our approach. When comparing the estimated Δt_{min} with the real elapsed time (we calculate the residual time as the difference between the real elapsed time and the estimated Δt_{min}), we observe a dependence with respect to the level of confidence levels (see histograms in Supplementary Figure 12). At 68% confidence level, the residual times show a clear overestimation (Supplementary Figure 12d), while at 99% confidence level, an underestimation is observed (Supplementary Figure 12b). However, the estimated minimum elapsed time fits pretty well with the real elapsed time at 95% of confidence level as shown in Supplementary Figure 12c (residuals follow a normal distribution centered at 0 yr). This result indicates that using a set of directional data that represents the "true" variation of the geomagnetic field at El Salt coordinates, our approach provides good results at 95% of confidence level but with a clear overestimation and underestimation for lower or higher confidence levels, respectively. Note that no relevant differences are observed between the estimated minimum elapsed time given by the three geomagnetic field models (SHA.DIF.14k, ArchKalMag14k, or Toy-Model). As expected, the Toy-model provides the lower Δt_{min} values, since this synthetic model was developed using the last 4000 yr, when the past geomagnetic field is well defined and directions present higher amplitude variability. However, the two paleoreconstructions (SHA.DIF.14k and ArchKalMag14k) cover the last 14000 yr and present smoother amplitude variabilities (see Pavón-Carrasco et al., 2014, Schanner et al., 2022, for more details).

Pair	**Angular deviation (º)**	**Real elapsed time (yr)**	**Estimated minimum elapsed time (yrs)**			
			Mode	**99%**	**95%**	**68%**
1	0.8	10	20 / 20 / 15	5 / 5 / 5	10 / 10 / 10	20 / 25 / 15
2	3.8	50	80 / 85 / 75	25 / 25 / 25	40 / 45 / 40	105 / 135 / 85
3	7.8	100	225 / 215 / 185	65 / 60 / 60	115 / 110 / 95	285 / 320 / 215
4	11.3	150	330 / 370 / 305	95 / 105 / 85	170 / 190 / 155	465 / 520 / 405
5	14.1	200	485 / 560 / 445	130 / 155 / 120	250 / 285 / 230	740 / 815 / 700
6	15.2	300	590 / 645 / 535	160 / 180 / 145	300 / 330 / 275	895 / 935 / 855

Supplementary Table 3. *Pair of directional data (column 1) with the angular deviation between directions (column 2). Real elapsed time (column 3) and estimated minimum elapsed time (columns 4 to 7) according to the approach for each pair of directional data. The estimated minimum elapsed time is given at four different statistical levels (mode, column 4; 99%: column 5; 95%, column 6; 68%, column 7). Results are provided for SHA.DIF.14k / ArchKalMag14k / Toy-model.*

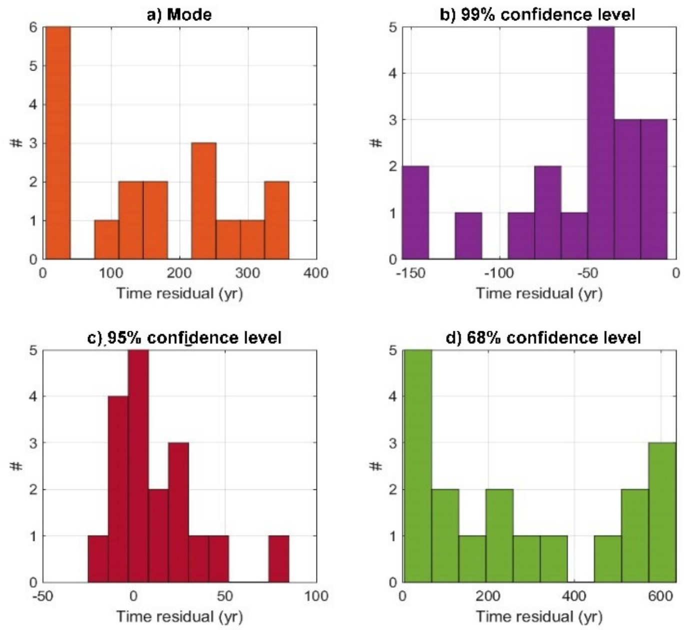

Supplementary Figure 12. *Histograms of the residual time calculated as the difference between the real elapsed time (column 3 in Supplementary Table 3) and the minimum elapsed time given by our approach at different confidence levels (columns 4 - 7 in Supplementary Table 3): A) Mode, B) 99 % confidence level, C) 95% confidence level, D) 68% confidence level. X-ayis indicates the number of data considered for the histograms.*

Case 2. Impact of the directional error (α_{95}) on the estimation of the Δt_{min}.

In this second case study, the directional dataset of Case 1 is utilized, with the addition of an α_{95} value for each direction ranging from 0º (results already provided in Case 1) to 6º (this range represents the common values of α_{95} for an archeomagnetic study). The objective is to introduce a directional error for each pair of directions to analyze how this error impacts on the estimation of the minimum elapsed times, taking into account that the minimum elapsed time is known a priori (the so-called real elapsed time).

Supplementary Figure 13 shows the results for the six directional pairs based on the α_{95} value and different levels of confidence: 68%, 95%, 99%, and the mode. As observed in all directional pairs, there are no significant differences observed based on the chosen paleoreconstruction (and toy-model). As for the Case 1, results indicate that the estimated minimum elapsed times are overestimated when using a 68% confidence level (yellow line) or the mode (blue line). However, they are underestimated when set at 99% (purple line). Consistent with Case 1, the 95% confidence level (red line) shows values closest to minimum real time (black dashed line). Another notable result is that for a specific pair, as α_{95} increases, no significant changes are observed in the estimation of minimum time for the 95% and 99% statistical levels. The most significant differences in relation to α_{95} occur at the mode and 68% statistical levels, where for real temporal times shorter than 150 years, the estimated minimum elapsed time increases, and for real temporal times greater than 150 years, the estimated minimum elapsed time decreases.

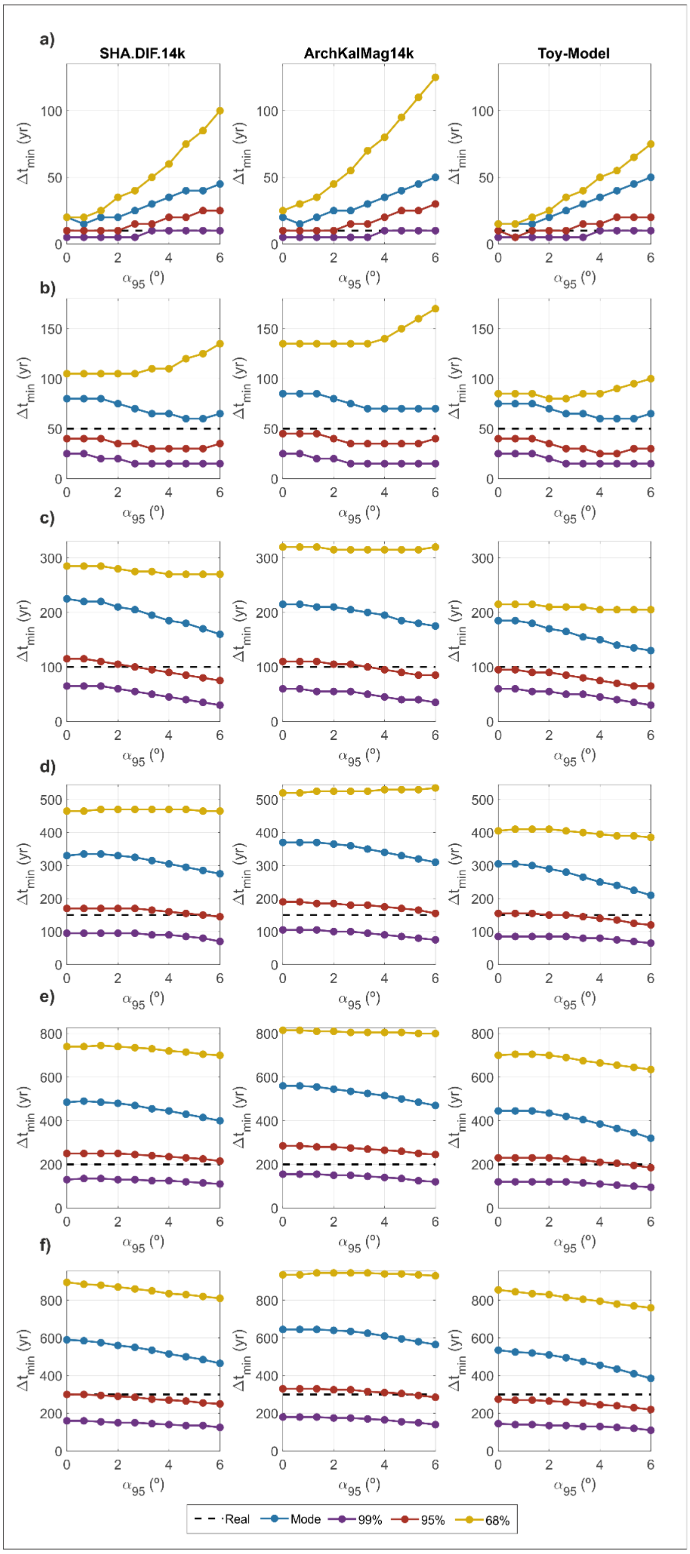

Supplementary Figure 13. *Estimated minimum elapsed time at different statistical levels (color lines; see legend) according to the two paleomagnetic reconstructions (SHA.DIF.14k, first column and ArchKalMag14k, second column) and the toy-model (third column). Black dashed lines show the real elapsed time for each pair of directional data: a) 10 yr; b) 50 yr; c) 100 yr; d) 150 yr; e) 200 yr; f) 300 yr.*

Case 3. Using archeomagnetic data with good time control and different ages. Directional data from combustion structures with good chronological control and clearly separated in time have been used to perform this test (Supplementary Table 4). Seven archeomagnetic directions were taken from the compilation of Gómez-Paccard *et al.*[57] and one from the study of Molina-Cardín *et al*.[26]. Since data within each pair come from different sites in Iberia and the method is implemented for El Salt site, directions have been relocated to El Salt coordinates for the test.

Two pairs of directions separated by ~200 years (PAR4-VIL2 & CALA-PATA; Supplementary Table 4) and two other pairs separated by ~1000 years (PATJ-EC5 & VIL1-CDAU; Supplementary Table 4) have been used to test the method. One of the two ~200-year pairs (PAR4-VIL2) presents a small angular deviation, and the other case (CALA-PATA) exhibits a larger angular deviation (Supplementary Table 5). These differences in the angular deviation are an expected consequence of the non-constant character or the SV rate of change (e.g. 150-350 CE *vs.* 1620-1820 CE; Supplementary Figure 2), i.e. the angular distance is not always the same for a given time difference. The same has been done for the ~1000-year pairs (PATJ-EC5, smaller angular deviation; VIL1-CDAU, larger angular deviation; Supplementary Table 5). This data selection has been done to assess the influence of differences of angular deviation in the estimated minimum elapsed times for pairs of directions with similar real elapsed times.

Real elapsed time between structures (column 2 of Supplementary Table 5) has been calculated considering the complete range of possible ages of each structure. For example, for pair PAR4-VIL2 (whose associated ages are 90-130 CE and 250-350 CE, respectively), the real elapsed time between them oscillates between 120 yrs (the minimum difference; between 130 CE and 250 CE) and 260 yrs (maximum difference; between 90 CE and 350 CE). Results of temporal estimations are summarized in Supplementary Table 5.

Comparing pairs with equivalent real elapsed times (PAR4-VIL2 *vs.* CALA-PATA and PATJ-EC5 *vs.* VIL1-CDAU), it is observed that differences in angular deviation values cause estimated minimum elapsed times to be unequal: the greater the angular distance, the greater the time difference. This is an expected result since the time estimation of our method is based on the magnitude of the angular deviation. Estimated minimum elapsed times at 95% and 99% of confidence are always below the range of real elapsed time (Supplementary Table 5). Mode is also below that range in most cases. In the case of 68% confidence level, most estimations fall within the range of real elapsed time (Supplementary Table 5). Overestimation is only detected in the mode and the 68% confidence level of the CALA-PATA pair. Although the results are quite acceptable in general terms, 99% and 95% confidence levels are the most conservative options in terms of minimum time.

Data ID	Mean age (yrs)	Age error (yrs)	Dating method	Dec In situ (º)	Inc In situ (º)	Dec El Salt (º)	Inc El Salt (º)	α_{95} (º)	Reference
PAR4	110 CE	±20	Archeol.	-2.7	53.3	-2.3	54.4	1.9	Gómez Paccard *et al* (2006)[57]
VIL2	300 CE	±50	Archeol.	-2.7	51.7	-2.2	49.8	2.2	Gómez Paccard *et al* (2006)[57]
CALA	1287.5	±12.5	Archaeol., Hist.	11.4	44.9	12.2	45.2	2.9	Gómez Paccard *et al* (2006)[57]
PATA	1475 CE	±25	Archeol.	3.6	56.4	3.6	55.6	1.7	Gómez Paccard *et al* (2006)[57]
PATJ	1520 CE	±91	^{14}C	6.6	62.2	6.5	61.5	1.1	Gómez Paccard et al (2006)[57]
EC5	525 CE	±25	^{14}C + Arch	3.5	59.1	3.6	56.4	3.1	Molina Cardín et al (2018)[26]
VIL1	50 CE	±50	Archeol.	-5.5	57.1	-5.2	55.4	2.6	Gómez Paccard et al (2006)[57]
CDAU	1116 CE	±87	^{14}C	9.6	45.7	8.8	41.8	1.3	Gómez Paccard et al (2006)[57]

Supplementary Table 4. *Dataset considered in Case 3: name of the data (column 1), age and error (columns 2-3), type of dating (column 4; Archeol. = archeological constrains; ^{14}C = ^{14}C radiocarbon dating; Hist. = historical constrains), declination [$Dec_{In\ situ}$] and inclination [$Inc_{In\ situ}$] in situ (columns 5-6), declination [$Dec_{El\ Salt}$] and inclination [$Inc_{El\ Salt}$] at El Salt coordinates (columns 7-8),* α_{95} *(column 9) and reference of data origin (column 10).*

Pair	Most probable angular deviation (º)	Real elapsed time (yrs)	Estimated minimum elapsed time (yrs)			
			Mode	99%	95%	68%
PAR4-VIL2	4.8	120-260	95/100/85	25/25/25	45/50/45	135*/165*/105
CALA-PATA	11.8	150-220	345/385/305	100/105/90	180/195/160	505/565/445
PATJ-EC5	5.5	879-1111	115/120/100	30/30/30	55/60/50	160/195/120
VIL1-CDAU	16.4	929-1203	655/785/595	175/215/160	335/395/310	1010*/1135*/975*

Supplementary Table 5. *Summary of the temporal estimations for the pairs of Case 3. Pair of directional data (column 1) with the angular deviation between directions (column 2). Real elapsed time (column 3) and estimated minimum elapsed time (columns 4 to 7) according to the approach for each pair of directional data. The estimated minimum elapsed time is given at four different statistical levels (mode, column 4; 99%: column 5; 95%, column 6; 68%, column 7). Results are provided for SHA.DIF.14k / ArchKalMag14k / Toy-model. Estimates marked with * indicate that they are within the range of the real elapsed time.*

Case 4. Using archeomagnetic data of the same age context. Directional data from "contemporaneous" combustion structures have been used to perform this test (Supplementary Table 6). Our method should not be applied to strictly coeval materials, since it is expected that the inherent uncertainties associated with the archeomagnetic data will commonly lead to an overestimation of the estimated minimum elapsed time. Nevertheless, these tests are used to analyse how much the angular deviations between them would influence the estimated minimum elapsed time in those cases. Considering different scenarios, three datasets taken from Osete et al.20, Molina-Cardín et al.26 and Herrejón-Lagunilla et al.31 have been used for the test:

A) Directional data of three structures from Tossal de la Vila (Castelló, Spain) (from Osete *et al.*[20]): TOS1, TOS2, TOS3. There is no independent dating for each structure individually, but they were considered contemporaneous because they are within the same archeological context. There are significant angular differences between some of these data.

B) Directional data of two structures from different sites but with a similar age (from Molina-Cardín *et al.*[26]): EC5 (El Castillón, Zamora, Spain) and OT (Cerro de los Almadenes, Otero de Herreros, Segovia, Spain). Angular deviation between EC5 and OT is not great.

C) Directional data from three experimental fires carried out in 2010 in the surrounding area of El Salt (published by Herrejón-Lagunilla *et al.*[31]): NFT-9, NFT-18 and NFT-22. They are open-air fires experimentally recreated in 2010 under controlled conditions (including some intentional post-burn actions) and abandoned for 5 years until their excavation and sampling. Their degree of preservation is variable. Angular deviations in this case are presumably caused (at least in part) by taphonomic processes.

The directions of datasets A) and B) have been relocated to El Salt site to perform the test. Dataset C) was not relocated because it comes from El Salt area.

Structure ID	**Mean age (yrs)**	**Age error (yrs)**	**Dating method**	**Dec** In situ **(º)**	**Inc** In situ **(º)**	**Dec** El Salt **(º)**	**Inc** El Salt **(º)**	**α_{95} (º)**	**Reference**
TOS1	775 CE	±25	^{14}C + Arch	11.3	68.1	11.1	66.9	2.4	Osete *et al.* (2020)[20]
TOS2	775 CE	±25	^{14}C + Arch	17.3	57.9	16.9	56.4	6.7	Osete *et al.* (2020)[20]
TOS3	775 CE	±25	^{14}C + Arch	10.5	55.1	10.2	53.5	3.7	Osete *et al.* (2020)[20]
EC5	525 CE	±25	^{14}C + Arch	3.5	59.1	3.6	56.4	3.1	Molina Cardín *et al.* (2018)[26]
OT	529 CE	±86	TL	-2.0	59.3	-1.9	57.3	1.7	Molina Cardín *et al.* (2018)[26]
NFT-9	2010 CE	±0	Experim.	1.4	60.4	1.4	60.4	5.5	Herrejón Lagunilla *et al.* (2019)[31]
NFT-18	2010 CE	±0	Experim.	4.8	51.9	4.8	51.9	1.7	Herrejón Lagunilla *et al.* (2019)[31]
NFT-22	2010 CE	±0	Experim.	-10.8	52.6	-10.8	52.6	8.2	Herrejón Lagunilla *et al.* (2019)[31]

Supplementary Table 6. *Dataset considered in Case 4: name of the data (column 1), age and error (columns 2-3), type of dating (column 4; Archeol. = archeological constrains; 14C = 14C radiocarbon dating; Experim. = fires made experimentally on known dates), declination [$Dec_{In\ situ}$] and inclination [$Inc_{In\ situ}$] in situ (columns 5-6), declination [$Dec_{El\ Salt}$] and inclination [$Inc_{El\ Salt}$] at El Salt coordinates (columns 7-8),* α_{95} *(column 9) and reference of data origin (column 10).*

a) Tossal de la Vila dataset:

Results for Tossal de la Vila dataset are presented in Supplementary Table 7. There are non-negligible angular deviations between some of the directions of this dataset. Since our method is based on the magnitude of the angular deviations, the time difference will be greater in those materials with greater angular differences. As expected, the pair with the smallest angular deviation (TOS2-TOS3; most probable angular deviation = 5.8º; Supplementary Table 7) exhibits the lowest temporal differences.

It should be noted that there are not three independent datings -one for each structure- that are exactly coincident for TOS1, TOS2, TOS3. It was assumed from the archeological context that they must correspond to the same date (see supplementary materials of Osete et al. 2020 for further information). But it cannot be ruled out that there is a certain temporal difference between the last burning of each of these structures. This is the main problem that our work aims to address: archeological materials may appear in the same units or even paleosurfaces without necessarily corresponding to an exactly coinciding date (and it can happen in any context, not only in Palaeolithic deposits). Nevertheless, we assume the error associated with dating (50 years; Supplementary Table 6) as the maximum temporal difference between these three structures. Estimated minimum elapsed time of TOS2-TOS3 at 95% and 99% fall within the range of real elapsed time (Supplementary Table 7). Mode and 68% overestimates the time (although mode only exceeds in some decades). Estimated minimum elapsed times for TOS1-TOS2 and TOS1-TOS3 are greater, commonly exceeding a century. The great overestimation in these two pairs is related to the large angular deviation observed between the directions (>10º). This angular deviation is high for coeval records. It is likely related to the uncertainties/bias in the archeomagnetic data and/or the dating. It is worth noting that we have set the maximum time difference between structures based on the error of the single dating assigned to these materials. It would be necessary to have an independent dating for each structure to assess the real elapsed time in more detail. In any case, 2 of the 3 pairs (TOS2-TOS3 and TOS1-TOS2) show estimated minimum elapsed times at 99% in the magnitude order of the maximum real elapsed time (decades).

Pair	**Most probable angular deviation (º)**	**Real elapsed time (yrs)**	**Estimated minimum elapsed time (yrs)**			
			Mode	**99%**	**95%**	**68%**
TOS2-TOS3	5.8	0-50	80/90/75	15/20/15	40/45/35	155/190/115
TOS1-TOS2	11.1	0-50	275/305/215	75/75/65	145/155/120	435/495/355
TOS1-TOS3	13.5	0-50	420/475/370	115/130/105	220/245/200	655/725/600

Supplementary Table 7. *Summary of the temporal estimations for the pairs of Tossal de la Vila. Pair of directional data (column 1) with the angular deviation between directions (column 2). Real elapsed time (column 3) and estimated minimum elapsed time (columns 4 to 7) according to the approach for each pair of directional data. The estimated minimum elapsed time is given at four different statistical levels (mode, column 4; 99%: column 5; 95%, column 6; 68%, column 7). Results are provided for SHA.DIF.14k / ArchKalMag14k / Toy-model.*

b) EC5-OT

Here we test materials from different sites but the same (or at least as similar as possible) ages, independently contrasted. Although dating errors are not the same, the two directions used here come from materials whose mean age only differs by 4 years (Supplementary Table 6).

Results of this test are summarized in Supplementary Table 8. It can be observed that estimated minimum elapsed time is smaller than in Case 3A due to the smaller angular deviation here. If we consider the complete, possible age intervals for both materials (500-550 CE for EC5; 443-615 CE for OT; Supplementary Table 6) and calculate the real elapsed time between them (0-115 yrs), all the estimates always fall within that range. In fact, the estimate at 99% according to the toy-model (10 yrs; Supplementary Table 8) is very close to the difference between the mean ages of these structures (4 yrs).

Pair	Most probable angular deviation (º)	Real elapsed time (yrs)	Estimated minimum elapsed time (yrs)			
			Mode	99%	95%	68%
EC5-OT	3.4	0-115	55/55/50	15/15/10	25/30/25	85/105/65

Supplementary Table 8. *Summary of the temporal estimations for the pair EC5-OT from Molina-Cardín et al.*[26]*. Pair of directional data (column 1) with the angular deviation between directions (column 2). Real elapsed time (column 3) and estimated minimum elapsed time (columns 4 to 7) according to the approach for each pair of directional data. The estimated minimum elapsed time is given at four different statistical levels (mode, column 4; 99%: column 5; 95%, column 6; 68%, column 7). Results are provided for SHA.DIF.14k / ArchKalMag14k / Toy-model.*

c) Experimental dataset

Finally, we analyze three experimental hearths conducted in 2010 in the area of El Salt (presented in [31]). They were part of a set of several combustion structures that simulated different, controlled post-depositional conditions. The three fires were left outdoors for 5 years to analyze the taphonomic processes affecting them. The main goal was to assess how faithfully the Earth´s magnetic field direction was recorded in these hearths (subjected to different alteration processes), providing models to compare with the archeological ones. Due to the different controlled taphonomic conditions experimented by each hearth, preservation degree was variable. NFT9 was intensively trampled for 15 days after its extinction. A well-preserved hearth usually exhibits an ash facies overlying a black and/or rubified facies. NFT9 ashes were totally reworked (since they are the most likely to be remobilized) but the subjacent black layer remained *in situ*. NFT18 and NFT22 were not subjected to any post-burning intentional mechanical alteration. NFT22 was characterized by a black layer that was difficult to distinguish during sampling and excavation. This was interpreted as a possible low thermoalteration and/or poor preservation in some parts of it. In the case of NFT18, no evident macroscopic alterations were detected. Taphonomical processes documented included trampling, slight bioturbation and exposition to atmospheric agents.

Although the directional record of these experimental fires is quite acceptable, they have some disturbances likely due to taphonomic processes (see Discussion in [31]). Furthermore, estimated minimum times inferred with our method are expected to be usually overestimated when dealing with strictly coeval materials (due to the uncertainties associated with the archaeomagnetic). However, this dataset allows us to assess the estimated minimum elapsed times for structures affected by well-known taphonomic processes.

Estimated minimum elapsed times for the experimental dataset are shown in Supplementary Table 9. Angular deviations even greater than 10º are observed in this dataset. As expected, estimated minimum elapsed times are overestimated in all cases. Despite the overestimation, it should be noted that estimated minimum elapsed times at 99% never exceed 60 years (Supplementary Table 9). This is probably influenced to a large extent by the effects of the documented taphonomic processes in the archaeomagnetic record (although other sources of uncertainties -such as measurement or sampling uncertainties- may also be affecting). It is worth mentioning that the preservation conditions of these experimental fires are not necessarily the same as those of all the older archaeological hearths, since they recreate very specific processes. In any case, errors of a few decades in the estimates fall within the scale of a single human generation or a single human life, which would imply a very high resolution considering that this method is being applied to Paleolithic hearths older than 50 ky (even beyond the radiocarbon applicability).

Pair	**Most probable angular deviation (º)**	**Real elapsed time (yrs)**	**Estimated minimum elapsed time (yrs)**			
			Mode	**99%**	**95%**	**68%**
NFT9-NFT18	9.0	0	220/230/175	60/55/55	110/115/95	320/370/250
NFT18-NFT22	10.2	0	220/240/170	50/55/45	110/120/90	360/420/285
NFT9-NFT22	11.0	0	225/250/170	50/55/45	115/125/95	400/465/320

Supplementary Table 9. *Summary of the temporal estimations for the pairs of experimental dataset. Pair of directional data (column 1) with the angular deviation between directions (column 2). Real elapsed time (column 3) and estimated minimum elapsed time (columns 4 to 7) according to the approach for each pair of directional data. The estimated minimum elapsed time is given at four different statistical levels (mode, column 4; 99%: column 5; 95%, column 6; 68%, column 7). Results are provided for SHA.DIF.14k / ArchKalMag14k / Toy-model.*

LIMITATIONS OF THE METHOD AND INDICATIONS FOR FUTURE USERS.

The information presented above has shown that calculation methods work properly, albeit there are some issues to keep in mind when using our minimum time estimation method. They are summarized below:

a) Confidence level

Our tests have shown that when we use instrumental data (e.g. IGRF), the values that most closely match the temporal differences are those with a 95% of confidence level. The values at 99% underestimate, and the mode and 68% overestimate. However, when considering archeomagnetic data, confidence levels between 95 and 99% are recommended, since they are the most conservative option. These difference in the results are likely related to the difference in the type of data (geomagnetic reconstructions are based on direct measurement of the Earth's magnetic field, while archeomagnetic data provides an indirect measurement of the field with different error sources) and the differences in the level of variability of the Earth`s magnetic field depending on the chosen period (geomagnetic data come from the last 200 yrs and the Earth's magnetic field has changed rapidly in comparison with other periods [e.g. see Supplementary Figure 3 of the Supplementary Methods 2]). Mode or 68% of confidence level should not be used in any case, as their values are usually overestimated. Thus, confidence levels of 95-99% (and preferable 99% to do a more conservative interpretation in terms of minimum times) are those recommended to work with archeomagnetic data.

b) Preservation of the structures and taphonomic conditions

Taphonomical processes may affect the archeomagnetic record, which can lead to deviations in the mean directions. However, these processes are sometimes only detected in the laboratory. Sampling the maximum area possible, avoiding physically altered parts and selecting the best burned areas usually works well. Here we studied multiple hearths apparently well preserved in the field. However, we finally selected only those well-preserved (or parts of them), well-heated and not showing evidence of taphonomic alterations. Considering that we are dealing with Palaeolithic hearths, we only considered directional data with $N>6$, $k>50$ and $\alpha_{95}<10^{o}$. It is recommended to select only unaltered and well-heated combustion structures for archeomagnetic analyses. Applying other analyses such as soil micromorphology may also help to this aim.

c) Uncertainties inherent to the archeomagnetic record

Uncertainties inherent to the archeomagnetic record cannot totally be avoided. It can affect the temporal estimates, but they especially influence when the actual time differences are very small. For that reason, it does not make sense to apply the method to coeval records.

Sampling/subsampling and measurement errors are assumed to be stochastic and included in the uncertainty parameter α_{95} (a good strategy to average these errors is to collect as much samples as possible). As shown in Case 2, differences in α_{95} values can affect the estimations but they do not tend to strongly increase/decrease the minimum time estimates at confidence levels of 95% and 99%.

d) Models, time period and place considered for the temporal estimates

The selection of a model to carry out the temporal estimations is key for the final results, due to their different smoothing degree, and the type and temporal distribution of the materials used to generate the reconstructions. In our case, we used paleoreconstructions that only consider TRM data and that cover as much time as possible (for instance, the last 14000 yr). For that reason, the results were similar regardless of the reconstruction used. In the case of the toy-model, the results are not very different, but it is more conservative because it only considers the last 4000 yrs and does not take into account the older parts of the models (which tend to be more smoothed).

The method can only be applied to periods of geomagnetic stability. This means that moments associated to geomagnetic excursions or polarity inversions should be avoided, as the field is unstable. It should also be noted that secular variation is a process with a variable rate of change through time and its erratic nature (within certain directional limits for every region) may imply that the same direction of the Earth´s magnetic field may be repeated at different times. If the selected time range of the model used to estimate the minimum time is especially short (i.e.: a few centuries) or coincides with a moment where the direction of the geomagnetic field barely varies, it is likely that an overestimation will be obtained. For this reason, the selection of the temporal range of the models is also important. We have considered broad temporal ranges (14000 yrs for SHA.DIF.14k and ARCHKALMAG14k, 4000 yrs for the toy model) to cover periods as representative as possible.

Our method is designed to work in the coordinates of El Salt site (Spain). It could be applied to any other worldwide site but the probability density functions that relate angular deviations and estimated minimum elapsed times must be generated at those coordinates (see Supplementary Methods 2 for more details).

e) Final remarks

The application of this method to temporally dissect Paleolithic palimpsests with hearth assemblages is firstly based on the stratigraphic isolation of every hearth by archeostratigraphy. By analyzing the overlapping and/or lateral continuity of their facies is a first approximation to determine which hearth is earlier or later to another. Subsequently, the application of archeomagnetic analyses allows to determine their minimum time at certain confidence level. The method should not be applied to structures that are considered coeval, as in such cases it may overestimate the time difference because of the effect of the uncertainty of the archeomagnetic data.

Although the method does not give a single absolute value, the minimum time calculations determined with this method allow us to make a quantitative approximation of the order of magnitude in which the human occupations occurred. This is an important advance for the study of these contexts, due to the difficulty of obtaining a time frame for their human occupations.

The quality of the magnetic record is a fundamental factor in such old materials, but also getting reliable data from them makes them particularly valuable. The use of fire is relatively common in many sites for the last *ca*. 200.000 yrs[58], so this technique opens new ways to reconstruct the nature of the occupations of our ancestors.

f) About of the use of the program

README file containing instructions for using the program is included in the folder with the program (see Code Availability Statement). Furthermore, some informative comments are included in the program code. The program was developed with Matlab.

Additional references in Supplementary Information:

50. L. J. Pérez Luis, “Estrategias de subsistencia y dinámicas de asentamiento en los Valles de Alcoy durante el Paleolítico medio. Análisis zooarqueológico, tafonómico y paleoecológico de la secuencia arqueológica de El Salt (Alcoy, Alicante)”, thesis, Universitat Rovira i Virgili, Tarragona (2019).

51. L. J. Pérez, J. Machado, C. M. Hernández, J. V. Morales, J. P. Brugal, B. Galván, Arqueozoología y arqueoestratigrafía del yacimiento de El Salt (Alcoi, Alicante): contribución metodológica para el análisis del registro faunístico contenido en palimpsestos arqueológicos del paleolítico medio” in Preses petites i grups humans en el passat. II Jornades d’arqueozoologia del Museu de Prehistòria de València, A. Sanchís, J. L. Pascual, Eds. (Diputació de València, Museu de Prehistòria de València, 2015): pp. 223-244.

52. Á. Carrancho, Á. Herrejón Lagunilla, J. M. Vergès, Three archaeomagnetic applications of archaeological interest to the study of burnt anthropogenic cave sediments. Quaternary International 414, 244-257 (2016).

53. V. Aldeias, H. L. Dibble, D. Sandgathe, P. Goldberg, S. J. P. McPherron, How heat alters underlying deposits and implications for archaeological fire features: A controlled experiment. Journal of Archaeological Science 67, 64-79 (2016).

54. L. Tauxe, S.K. Banerjee, R.F. Butler, R. van der Voo, Essentials of Paleomagnetism, 5th Web Edition. https://earthref.org/MagIC/books/Tauxe/Essentials/ (2018)

55. A. Jackson, A. R. T. Jonkers, M. R. Walker, Four centuries of geomagnetic secular variation from historical records. Philosophical Transactions of the Royal Society A: Mathematical, Physical and Engineering Sciences 358 (1768), 957-990 (2000).

56. P. Alken, E. Thébault, C.D. Beggan, H. Amit, J. Aubert, J. Baerenzung, T.N. Bondar, W. Brown, S. Califf, A. Chambodut, A. Chulliat, G. Cox, C.C. Finlay, A. Fournier, N. Gillet, A. Grayver, M.D. Hammer, M. Holschneider, L. Huder, G. Hulot, T. Jager, C. Kloss, M. Korte, W. Kuang, A. Kuvshinov, B. Langlais, J.M. Léger, V. Lesur, P.W. Livermore, F.J. Lowes, S. Macmillan, J.E. Mound, M. Nair, S. Nakano, N. Olsen, F.J. Pavón-Carrasco, V.G. Petrov, G. Ropp, M. Rother, T.J. Sabaka, S. Sanchez, D. Saturnino, N.R. Schnepf, X. Shen, C. Stolle, A. Tangborn, L. Tøffner-Clausen, H. Toh, J.M Torta, J. Varner, F. Vervelidou, P. Vigneron, I. Wardinski, J. Wicht, A. Woods, Y. Yang, Z. Zeren, B. Zhou, International Geomagnetic Reference Field: the thirteenth generation. Earth Planets Space 73(49), 1–25 (2021).

57. M. Gómez-Paccard, G. Catanzariti, V. C. Ruiz-Martínez, G. McIntosh, J. I. Núñez, M. L. Osete, A. Chauvin, Ph. Lanos, D. H. Tarling, D. Bernal-Casasola, J. Thiriot, A. Sáez-Espligares, I. García-Villanueva, J.A. Gisbert-Santonja, M.A. Hervás, P. Jiménez-Castillo, M. Mesquida-García, I. Navarro, M. Orfila-Pons, I. Ramírez-González, M. Retuerce, D. Urbina, C. Urquijo, A catalogue of Spanish archaeomagnetic data. Geophysical Journal International 166, 1125–1143 (2006).

58. W Roebroks, P Villa, On the earliest evidence for habitual use of fire in Europe, Proceedings of the National Academy of Sciences of the United States of America 108 (13), 5209–5214 (2011)